1 Basic Theory

1.1 Interaction of Nuclei with External Magnetic Fields

The Hamiltonian for a nuclear spin $\boldsymbol{I}$, interacting with an external magnetic field $\boldsymbol{B}$ is

$$\mathcal{H} \;=\; -\gamma\,\hbar\,\boldsymbol{B}\cdot\boldsymbol{I}, \tag{1.01}$$

where $h \;=\; 2\pi\,\hbar$ denotes Planck's constant and γ is the gyromagnetic ratio; see Abragam [1]. For the case of a static external magnetic field $\boldsymbol{B_0}$ pointing in the z-direction of the laboratory frame we have

$$\mathcal{H}_{\mathrm{L}} \;=\; -\gamma\,\hbar\,B_0\cdot I_z, \tag{1.02}$$

and, with the definition of the Larmor frequency,

$$\boldsymbol{\omega}_{\mathrm{L}} \;=\; -\gamma\,\boldsymbol{B}_0\,. \tag{1.03}$$

The gyromagnetic ratios for the chemical shift reference materials of all NMR isotopes were fixed by the IUPAC convention in 2001 [2]. Therefore, the Larmor frequency is in strict terms the frequency of the reference signal, e. g., of the tetramethylsilane signal for ^{1}H, ^{13}C and ^{29}Si nuclei. However, often the term "Larmor frequency" is generally used for the resonance frequency of any single NMR signal at the given external magnetic field.

Eq. (1.02) can be rewritten as

$$\mathcal{H}_{\mathrm{L}} \;=\; \hbar\,\omega_{\mathrm{L}}\,I_z. \tag{1.04}$$

A radio frequency field RF in the y-direction with the angular frequency ω (which is close to the Larmor frequency ω_{L} and to the pulse carrier frequency ω_{c}; see Section 1.3),

$$B_y(t) \;=\; 2\,B_{\mathrm{RF}}\cos(\omega\,t), \tag{1.05}$$

enlarges the Hamiltonian

$$\mathcal{H}_{\mathrm{L}} \;=\; \hbar\,\omega_{\mathrm{L}}\;I_z \;+\; 2\,\hbar\,\omega_{\mathrm{RF}}\,I_z\cos(\omega\,t)\,I_y, \tag{1.06}$$

where ω_{RF} is defined as the nutation frequency

$$\boldsymbol{\omega}_{\mathrm{RF}} \;=\; -\gamma\,\boldsymbol{B}_{\mathrm{RF}}. \tag{1.07}$$

Sometimes the vector equations above, which distinguish between a clockwise and negative rotation for positive γ and counterclockwise and positive rotation for negative γ, are simplified to consider positive frequencies only:

$$\omega_{\mathrm{L}} \;=\; |\gamma|\,B_0 \text{ or } \nu_{\mathrm{L}} \;=\; \omega_{\mathrm{L}}/2\pi \text{ and } \omega_{\mathrm{RF}} \;=\; |\gamma|\,B_{\mathrm{RF}} \text{ or } \nu_{\mathrm{RF}} \;=\; \omega_{\mathrm{RF}}/2\pi. \tag{1.08}$$

However, all signs, beginning with the sign of the Larmor rotation, should be consistently considered for advanced NMR experiments [3].

1.2 Irreducible Tensor Operator Calculus

It is useful to express the internal interactions of a nuclear spin in the notation of irreducible tensor operators; see Weissbluth [4]. If $T_m^{(k)}$ denotes one of the $(2k+1)$ components of an irreducible tensor operator of rank k, then it is transformed under a coordinate rotation, $\boldsymbol{r} = \boldsymbol{r}'R$, to

$$P_R T_m^{(k)} P_R^{-1} = \sum_{m'} T_{m'}^{(k)} D_{m'm}^{(k)}(R), \qquad m, m' = k, k-1, \ldots, -k, \tag{1.09}$$

where $D_{m'm}^{(k)}(R)$ denotes the matrix elements of the irreducible representation $D^{(k)}$ of the group of ordinary three-dimensional rotations (Wigner D-Matrix [5]). We use here the index m in agreement with the majority of the literature. It is not generally identical to the magnetic quantum number m. The transformation operator P_R is given by

$$P_\mathrm{R} = \exp(\mathrm{i}\,\Omega\,\boldsymbol{n}\cdot\boldsymbol{J}), \tag{1.10}$$

where $\boldsymbol{J}$ is the total angular momentum operator, $\boldsymbol{n}$ is the unit vector pointing in the direction of rotation, and Ω represents the angle of rotation. Such a rotation transforms the eigenfunctions, $|Im\rangle$, of the angular momentum operator I_z of a nuclear spin $\boldsymbol{I}$, as

$$P_\mathrm{R}|Im\rangle = \sum_{m'} |Im'\rangle D_{m'm}^{(I)}(R), \tag{1.11}$$

where $D_{m'm}^{(I)}$ denotes the Wigner D-matrix. The Wigner D-matrix can be rewritten by means of Wigner's small d-matrix (also called the "reduced real" Wigner Matrix) $d_{m'm}^{(k)}(\beta)$:

$$D_{m'm}^{(k)}(\alpha,\beta,\gamma) = \exp(-\mathrm{i}\,m'\,\alpha)\; d_{m'm}^{(k)}(\beta)\; \exp(-\mathrm{i}\,m\gamma). \tag{1.12}$$

Table 1.1 gives values of the D-Matrix for ranks $k = 1/2$ and $k = 2$. The d-matrix elements from rank ½ up to rank 5 can be found in the textbook of Varshalovitch *et al*. [6], where M and M' are used instead of m' and m, respectively. Eq. (1.12) is the most common relation between the D- and d-matrices [7]. A slightly different form using plus instead of minus signs in Eq. (1.12) holds for Euler angles on the base of the left-hand screw rule [4, 5] and was given in our previous review [8]. The different conventions of the Euler angles were compared by Goldstein *et al*. [7] and Morris and Parker [9]. A detailed description of active and passive rotations with Euler angles in NMR was recently presented by Man [10]. Currently, the most common conventions [7] employ the right-hand screw rule for the angle directions and are termed $z - x' - z''$ and $z - y' - z''$. We use the latter of these two conventions [11].

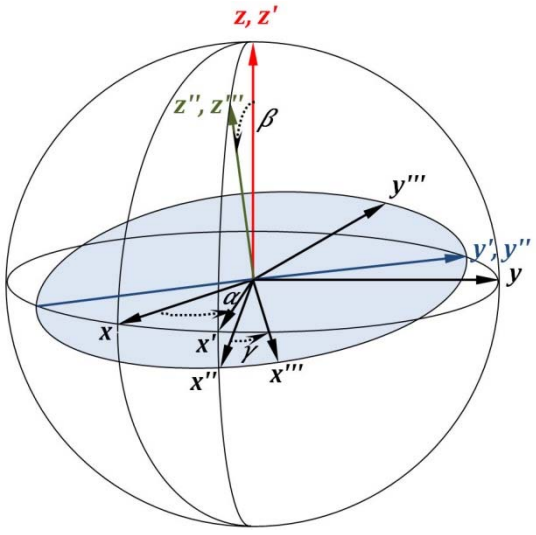

As presented in Fig. 1.1, a transformation of the frame (x, y, z) to the frame (x'', y'', z'') by Euler angles includes the rotation α about the original z axis, the rotation β about the obtained y' axis, and the rotation γ about the final z'' axis.

Fig. 1.1. Definition of the Euler angles corresponding to the right-hand screw rule for angles rotating around the z-, y'-, and z''-axes. .

Table 1.1. Wigner D-Matrix elements for rank k = ½ and k = 2.

$k = ½$	$m = ½$	$m = -½$
$m' = ½$	$\cos\frac{\beta}{2}\,e^{-\frac{\alpha+\gamma}{2}}\,e$	$\sin\frac{\beta}{2}e^{-\frac{\alpha-\gamma}{2}}$
$m' = -½$	$\sin\frac{\beta}{2}e^{-\frac{-\alpha+\gamma}{2}}$	$\cos\frac{\beta}{2}e^{-\frac{-\alpha-\gamma}{2}}$

$k = 2$	$m = 2$	$m = 1$	$m = 0$	$m = -1$	$m = -2$
$m' = 2$	$\frac{(1+\cos\beta)^2}{4}e^{-i(2\alpha+2\gamma)}$	$-\frac{\sin\beta(1+\cos\beta)}{2}e^{-i(2\alpha+\gamma)}$	$\sqrt{\frac{3}{8}}\sin^2\beta\,e^{-i(2\alpha)}$	$-\frac{\sin\beta(1-\cos\beta)}{2}e^{-i(2\alpha-\gamma)}$	$\frac{(1-\cos\beta)^2}{4}e^{-i(2\alpha-2\gamma)}$
$m' = 1$	$\frac{\sin\beta(1+\cos\beta)}{2}e^{-i(\alpha+2\gamma)}$	$\frac{2\cos^2\beta+\cos\beta-1}{2}e^{-i(\alpha+\gamma)}$	$-\sqrt{\frac{3}{2}}\sin\beta\cos\beta\,e^{-i(\alpha)}$	$-\frac{2\cos^2\beta-\cos\beta-1}{2}e^{-i(\alpha-\gamma)}$	$-\frac{\sin\beta(1-\cos\beta)}{2}e^{-i(\alpha-2\gamma)}$
$m' = 0$	$\sqrt{\frac{3}{8}}\sin^2\beta\,e^{-i(2\gamma)}$	$\sqrt{\frac{3}{2}}\sin\beta\cos\beta\,e^{-i(\gamma)}$	$\frac{3}{2}(\cos^2\beta-1)$	$-\sqrt{\frac{3}{2}}\sin\beta\cos\beta\,e^{-i(-\gamma)}$	$\sqrt{\frac{3}{8}}\sin^2\beta\,e^{-i(-2\gamma)}$
$m' = -1$	$\frac{\sin\beta(1-\cos\beta)}{2}e^{-i(-\alpha+2\gamma)}$	$-\frac{2\cos^2\beta-\cos\beta-1}{2}e^{-i(-\alpha+\gamma)}$	$\sqrt{\frac{3}{2}}\sin\beta\cos\beta\,e^{-i(-\alpha)}$	$\frac{2\cos^2\beta+\cos\beta-1}{2}e^{-i(-\alpha-\gamma)}$	$-\frac{\sin\beta(1+\cos\beta)}{2}e^{-i(-\alpha-2\gamma)}$
$m' = -2$	$\frac{(1-\cos\beta)^2}{4}e^{-i(-2\alpha+2\gamma)}$	$\frac{\sin\beta(1-\cos\beta)}{2}e^{-i(-2\alpha+\gamma)}$	$\sqrt{\frac{3}{8}}\sin^2\beta\,e^{-i(-2\alpha)}$	$\frac{\sin\beta(1+\cos\beta)}{2}e^{-i(-2\alpha-\gamma)}$	$\frac{(1+\cos\beta)^2}{4}e^{-i(-2\alpha-2\gamma)}$

A definition of an irreducible tensor operator that is equivalent to Eq. (1.09) is given by the commutators [4]. If instead of the total angular momentum operator $\boldsymbol{J}$ only the nuclear spin $\boldsymbol{I}$ is concerned, we have

$$\left[I_0, T_m^{(k)}\right] = q\, T_m^{(k)}, \qquad \left[I_{\pm 1}, T_m^{(k)}\right] = \mp\sqrt{\{k(k+1) - m(m \pm 1)\}/2}\; T_{m\pm 1}^{(k)} \tag{1.13}$$

with

$$I_0 = I_z, \qquad I_{\pm 1} = \mp\, I_\pm/\sqrt{2}, \quad \text{and} \quad I_\pm = I_x \pm \mathrm{i} I_y. \tag{1.14}$$

The tensor product, $U_Q^{(k)}$, of two operators with the components $T_m^{(k')}$ and $V_{m'}^{(k')}$ is defined as [4]

$$U_Q^{(k)} = \sum_{m,m'} T_m^{(k')} V_{m'}^{(k')} \langle kk'mm'|kk'KQ\rangle \tag{1.15}$$

The term $\langle kk'mm'|kk'KQ\rangle$ introduces the Clebsch-Gordan coefficients [6]. $U_Q^{(k)}$ is an irreducible tensor operator. $U_0^{(0)}$ is the scalar component of that tensor operator and, given the properties of the Clebsch-Gordan coefficients, it is found that

$$U_0^{(0)} = \frac{(-1)^k}{\sqrt{2k+1}} \sum_m (-1)^m T_m^{(k)} V_{-m}^{(k)}, \qquad m = -k, -k+1, \ldots, +k. \tag{1.16}$$

Most interactions in NMR can be written in this form [12]. It is important that the operators $T_m^{(k)}$ and $T_m^{(k)} V_{-m}^{(k)}$ mostly act on two different non-interacting systems, the nuclear spin coordinates and spatial coordinates (framework parameters), respectively. Irreducible tensor calculus is most useful when coordinate transformations have to be considered, as in the case of the transformation to the principle axis system (PAS) of a tensor, e.g., for the description of sample spinning.

1.3 Rotating Frame

NMR spectrometers use RF pulses with a carrier frequency ω_c near the Larmor frequency ω_L, perform a phase sensitive detection and a Fourier transform, and provide a signal at the resonance offset $\Delta\omega = \omega_\mathrm{L} - \omega_\mathrm{c}$. Therefore, it is most useful to perform a transition into a frame rotating with an angular frequency ω_c by separating out the Hamiltonian $\mathcal{H}_0 = \hbar\omega_\mathrm{c} I_z$.

The total Hamiltonian in the Schrödinger representation can be written as $\mathcal{H}(t) = \mathcal{H}_0 + \mathcal{H}_1(t)$. To switch from the Schrödinger representation (s) to the interaction representation (i), the wave function $|\phi_\mathrm{s}\rangle$ and any operator A_s must be transformed by the unitary operator

$$P_\mathrm{i} = \exp\left[\frac{\mathrm{i}}{\hbar}\mathcal{H}_0(t - t_0)\right], \tag{1.17}$$

so that [13]

$$|\phi_\mathrm{i}\rangle = P_\mathrm{i}|\phi_\mathrm{s}\rangle, \qquad A_\mathrm{i}(t) = P_\mathrm{i} A_\mathrm{s} P_\mathrm{i}^{-1}. \tag{1.18}$$

The equations of motion for the wave function and the density operator ρ_i in the interaction representation are [13]

$$\frac{\partial}{\partial t}|\phi_\mathrm{i}\rangle = -\frac{\mathrm{i}}{\hbar}\mathcal{H}_{1,\mathrm{i}}|\phi_\mathrm{i}\rangle, \qquad \frac{\partial}{\partial t}\rho_\mathrm{i} = -\frac{\mathrm{i}}{\hbar}\left[\mathcal{H}_{1,\mathrm{i}}, \rho_\mathrm{i}\right]. \tag{1.19}$$

Using $\mathcal{H}_0 = \hbar\omega_\mathrm{c} I_z$, and the resonance offset $\Delta\omega = \omega_\mathrm{L} - \omega_\mathrm{c}$, we have for the Hamiltonian in the interaction representation, according to Eq. (1.17),

$$\mathcal{H}_{1,\mathrm{i}} = \hbar\,\Delta\omega\, I_z + \exp(\mathrm{i}\omega_\mathrm{c} I_z t)\,\mathcal{H}_1 \exp(-\mathrm{i}\omega_\mathrm{c} I_z t). \tag{1.20}$$

A formal solution to the equation of motion of the density operator, Eq. (1.19), is obtained by the unitary evolution operator $U_\mathrm{i}(t, t_0)$:

$$\rho_\mathrm{i}(t) = U_\mathrm{i}(t, t_0)\rho_\mathrm{i}(t_0)U_\mathrm{i}(t, t_0)^{-1}. \tag{1.21}$$

The evolution operator $U_\mathrm{i}(t, t_0)$ obeys the equation

$$\frac{\partial}{\partial t}U_\mathrm{i}(t, t_0) = -\frac{\mathrm{i}}{\hbar}\mathcal{H}_{1,\mathrm{i}}U_\mathrm{i}(t, t_0). \tag{1.22}$$

If the operator $\mathcal{H}_{1,\mathrm{i}}$ is time-independent, the solution is

$$U_\mathrm{i}(t, t_0) = \exp\left\{-\frac{\mathrm{i}}{\hbar}\mathcal{H}_{1,\mathrm{i}}(t - t_0)\right\}. \tag{1.23}$$

The general solution to Eq. (1.22) employs the Dyson time-ordering operator, $\mathcal{T}$ [14]:

$$U_\mathrm{i}(t, t_0) = \mathcal{T}\,\exp\left\{-\frac{\mathrm{i}}{\hbar}\int_{t_0}^{t}\mathcal{H}_{1,\mathrm{i}}(t, t_0)\mathrm{d}t_1\right\}. \tag{1.24}$$

The **Magnus expansion** [15] can be used in order to describe the evolution of a time-dependent, but periodic Hamiltonian, $\mathcal{H}_{1,\mathrm{i}}(t + Nt_\mathrm{c}) = \mathcal{H}_{1,\mathrm{i}}(t)$ with integer N:

$$U_\mathrm{i}(t, t_0 = 0) = \exp\left\{-\frac{\mathrm{i}}{\hbar}t_\mathrm{c}\left(\overline{\mathcal{H}^{(0)}} + \overline{\mathcal{H}^{(1)}} + \overline{\mathcal{H}^{(2)}} + \cdots\right)\right\}, \tag{1.25}$$

where

$$\overline{\mathcal{H}^{(0)}} = \frac{1}{t_\mathrm{c}}\int_0^{t_\mathrm{c}}\mathcal{H}_{1,\mathrm{i}}(t)\;\mathrm{d}t, \qquad \overline{\mathcal{H}^{(1)}} = \frac{-\mathrm{i}}{2t_\mathrm{c}}\int_0^{t_\mathrm{c}}\mathrm{d}t_2\int_0^{t_2}\mathrm{d}t_1\left[\mathcal{H}_{1,\mathrm{i}}(t_2), \mathcal{H}_{1,\mathrm{i}}(t_1)\right], \tag{1.26}$$

and the odd terms disappear for $\mathcal{H}_{1,\mathrm{i}}(t_\mathrm{c} - t) = \mathcal{H}_{1,\mathrm{i}}(t)$. For higher-order terms see [12].

The Hamiltonian for the static field in the z-direction is in the rotating frame instead of the laboratory axis system (LAB), see Eq. (1.04),

$$\mathcal{H}_{\mathrm{L,i}} = \hbar\,\Delta\omega\, I_z, \text{ where } \Delta\omega = \omega_\mathrm{L} - \omega_\mathrm{c}. \tag{1.27}$$

The y-pulse of the magnetic RF field corresponds to

$$\mathcal{H}_{\mathrm{RF,i}} = \hbar\omega_\mathrm{RF}\left[I_y\left(1 + \cos 2\omega_\mathrm{c} t + I_y \sin 2\omega_\mathrm{c} t\right)\right], \tag{1.28}$$

which, neglecting the time-dependent part, reduces to

$$\mathcal{H}_{\mathrm{RF,i}} = \hbar\omega_\mathrm{RF}\, I_y\,. \tag{1.29}$$

If ϕ is the phase difference of the pulse with respect to the y-direction, positive for a right-handed screw in the positive direction along the axis of rotation, one has from Eq. (1.10)

$$\mathcal{H}_{\mathrm{RF,i}} = \hbar\omega_\mathrm{RF}\exp\left(-\mathrm{i}\phi I_z\right) I_y \exp\left(+\mathrm{i}\phi I_z\right). \tag{1.30}$$

1.4 Free Induction Decay (FID) and Line Shape

By means of phase-sensitive quadrature detection, the demodulated free induction decay (FID) is digitized into two sets of data where a unique time difference between the two sets corresponds to a 90° phase shift of the carrier frequency of the RF pulse. Thus, the FID is a complex voltage and can be calculated as the relaxation function

$$G(t) \sim \frac{\mathrm{tr}\{\rho_\mathrm{i}(t) I_+\}}{\mathrm{tr}\{\rho\}} \equiv \frac{\langle I_- | \rho_\mathrm{i}(t)\rangle}{\langle \hat{1} | \rho\rangle}, \tag{1.31}$$

with $\hat{1}$ being the unity operator [1, 14].

The **high-temperature approximation**, $\|\mathcal{H}_\mathrm{L}\| \ll kT$, and the Magnus expansion were introduced [12] to achieve a density operator proportional to I_z for a single spin I. The obtained convention is

$$|\rho_0\rangle = |I_z\rangle. \tag{1.32}$$

Then the FID is given by

$$G(t) = \frac{\mathrm{tr}\{\rho_\mathrm{i}(t) I_+\}}{\mathrm{tr}\{I_x^2\}} \equiv \frac{\langle I_- | \rho_\mathrm{i}(t)\rangle}{\langle I_x | I_x\rangle} = \frac{\langle I_- | U_\mathrm{i}(t,t_0)\rho_\mathrm{i}(t_0) U_\mathrm{i}(t,t_0)^{-1}\rangle}{\langle I_x | I_x\rangle}. \tag{1.33}$$

See also Eq. (1.21), where $\rho_\mathrm{i}(t_0)$ represents the density operator after the pulse, $t_0 = 0$. As a good approximation, one can consider only operators in $U_\mathrm{i}(t)$, which are secular with respect to the Zeeman interaction. With

$$W_m = \tfrac{1}{2}\sqrt{I(I+1) - m(m+1)} = \tfrac{1}{2}\sqrt{(I-m)(I+m+1)} \tag{1.34}$$

(looking ahead to Eq. (2.23)), we find for Eq. (1.33):

$$G(t) = \frac{1}{\mathrm{tr}\{I_x^2\}} \sum_{m=-I}^{I-1} 2W_m \rho_{m,m+1} U_{m,m} U_{m+1,m+1}^{-1}. \tag{1.35}$$

It should be mentioned that in the present review the transition $m \to m+1$ is considered. One also finds the transition $m-1 \to m$ in the literature, with the central transition being $m = +\frac{1}{2}$. The two notations are essentially the same despite the difference in the signs of their imaginary parts.

The transverse relaxation time, T_2, is an important parameter for the characterization of the free induction decay. It is commonly defined as the time difference, $t_{1/\mathrm{e}}$, between the maximum initial value $G_\mathrm{max}(t=0)$ and the value $G_{1/\mathrm{e}}(t_{1/\mathrm{e}}) = G_\mathrm{max}/\mathrm{e}$, where e is the base of the natural logarithm.

The Fourier transform of the relaxation function $G(t)$ gives the line shape function $F(\Omega)$:

$$F(\Omega) = \int_{-\infty}^{+\infty} G(t) \exp\{-\mathrm{i}\Omega t\}\, \mathrm{d}t. \tag{1.36}$$

Since $U_\mathrm{i}(t) = \exp\left\{-\frac{\mathrm{i}}{\hbar}\mathcal{H}_\mathrm{i} t\right\}$ is diagonal in the set $|m\rangle$, we obtain for the observed signal

$$F(\Omega) = \frac{1}{\mathrm{tr}\{I_x^2\}} \sum_{m=-1}^{I-1} 2W_m \rho_{m,m+1}\, \delta\{\Omega - (\mathcal{H}_{\mathrm{m+1,m+1}} - \mathcal{H}_{\mathrm{m,m}})/\hbar\}. \tag{1.37}$$

We have $\Omega = \omega - \omega_{\mathrm{L}}$ and $\frac{(\mathcal{H}_{\mathrm{m+1,m+1}} - \mathcal{H}_{\mathrm{m,m}})}{\hbar} = \omega_{m+1,m} - \omega_{\mathrm{L}}$. The different interactions, $\mathcal{H}_{\mathrm{i}}$, generate the frequency distribution. The elements of the density operator, $\rho_{m,m+1}$, contain the information about the excitation; see Section 2.

An important parameter of the broadening of the line shape, $F(\Omega)$, in solid-state NMR spectra of powder materials is the second moment. We express the second moment as an integral over the spectral range

$$M_2 = \int \left(\Omega - \omega_{\mathrm{cg}}\right)^2 F(\Omega)\mathrm{d}\Omega. \tag{1.38}$$

The normalization of the line shape function,

$$M_0 = \int F(\Omega)\mathrm{d}\Omega = 1, \tag{1.40}$$

and the definition of the first moment,

$$M_1 = \int \left(\Omega - \omega_{\mathrm{cg}}\right) F(\Omega)\mathrm{d}\Omega = 0, \tag{1.39}$$

were used in Eq. (1.38).

The center of gravity is shifted with respect to the Larmor frequency by contributions from isotropic shifts like isotropic chemical shifts or isotropic second-order quadrupole shifts. The dimension of the second moment is s^{-2}. It changes to Hz^2 or T^2 if the line shape is given as $F(\nu)$ or $F(B)$, respectively. The corresponding dimensionless equation is $M_2(\Omega)/\mathrm{s}^{-2} = (1/2\,\pi)^2\, M_2(\nu)/\mathrm{Hz}^2 = \gamma_{\mathrm{I}}^2\, M_2(B)/\mathrm{T}^2$ for a correspondingly changed normalization in Eq. (1.40). It should be noted that for a Lorentzian line shape

$$F_{\mathrm{Lorentz}}(\Omega) = \frac{\delta}{\pi}\,\frac{1}{\delta^2 + \Omega^2}\ , \tag{1.41}$$

the second moment increases to an infinite value with increasing bounds of integration. The *half width at half intensity*, δ, is defined as angular frequency by [1]

$$F(\omega_{\mathrm{L}} + \delta) = \tfrac{1}{2} F(\omega_{\mathrm{L}}). \tag{1.42}$$

But the *full width at half maximum* (*fwhm*) is commonly used now as a measure for the line width. The $fwhm \equiv \delta\nu_{1/2}$ is defined by

$$F\left(\nu_{\mathrm{L}} \pm \tfrac{1}{2}\delta\nu_{1/2}\right) = \tfrac{1}{2} F(\nu_{\mathrm{L}}). \tag{1.43}$$

The relation to the line width parameter δ in Eq. (1.41) is $\delta = \pi\,\delta\nu_{1/2}$. A Lorentzian line shape corresponds to a single-exponential decay of the relaxation function $G(t) = \exp\frac{-t}{T_2}$ with the transverse relaxation time T_2. The frequency and time domain are connected by

$$\delta = \frac{1}{T_2} \qquad \text{or} \qquad \delta\nu_{1/2} = \frac{1}{\pi\, T_2}. \tag{1.44}$$

For the Gaussian line shape

$$F_{\mathrm{Gauss}}(\Omega) = \frac{1}{\sqrt{2\pi M_2}} \exp\frac{-\Omega^2}{2M_2}\ , \tag{1.45}$$

knowledge of the second moment provides the exact line width, in theory. It is $\delta = \sqrt{M_2 \ln 4}$ [1] or, for the *fwhm* given in Hz and M_2 provided in s^{-2},

$$\frac{\delta\nu_{1/2}}{\mathrm{Hz}} = \sqrt{\frac{\ln 4}{\pi^2}}\sqrt{\frac{M_2}{\mathrm{s}^{-2}}} \approx 0.375\sqrt{\frac{M_2}{\mathrm{s}^{-2}}}. \tag{1.46}$$

It is possible to obtain a rough estimation of the line broadening of a signal by assuming a Gaussian line shape and using Eq. (1.46). Equations for the calculation of second moments for different interactions will be given in the next sections.

1.4 Electric Quadrupole Interaction

We have two values describing the traceless electric field gradient tensor ($V_{XX} + V_{YY} + V_{ZZ} = 0$) in the principle axis system, PAS, with upper-case coordinates (X, Y, Z):

$$V_{ZZ} = eq, \;\; \eta = \frac{V_{XX} - V_{YY}}{V_{ZZ}}. \tag{1.47}$$

The asymmetry, η, of the electric field gradient is in the range $0 \leq \eta \leq 1$, if we label the axis so that $|V_{ZZ}| \geq |V_{YY}| \geq |V_{XX}|$. Additional explanations will be given after Eq. (1.94). The value q is exclusively used in a product with the elementary charge e. The Hamiltonian of the electric quadrupole interaction, as presented by Abragam [1] page 232, is

$$\mathcal{H}_\mathrm{Q} = \frac{e^2qQ}{4I(2I-1)}\left[3I_Z^2 - I(I+1) + \frac{1}{2}\eta(I_+^2 + I_-^2)\right] = \frac{e^2qQ}{4I(2I-1)}[3I_Z^2 - I(I+1) + \eta(I_X^2 - I_Y^2)]. \tag{1.48}$$

Q is the quadrupole moment, and eQ is called the electric quadrupole moment. The quadrupole coupling constant, C_Q, is commonly defined with Planck's constant h as

$$C_\mathrm{Q} = \frac{e^2qQ}{h}. \tag{1.49}$$

The quadrupole frequency, ν_Q or ω_Q, is defined by Abragam, see [1] (page 233), as

$$\nu_\mathrm{Q} = \frac{3e^2qQ}{2I(2I-1)h} = \frac{3\,C_\mathrm{Q}}{2I(2I-1)} \quad \text{or} \quad \omega_\mathrm{Q} = \frac{3e^2qQ}{2I(2I-1)\hbar} = \frac{3\pi\,C_\mathrm{Q}}{I(2I-1)}. \tag{1.50}$$

It can be seen in Fig. 1.2 that for $\eta = 0$ the quadrupole frequencies ν_Q and ω_Q correspond to the frequency distance between the singularities in the powder pattern for the $\pm 3/2 \leftrightarrow \pm 1/2$ transitions. This is equal to the maximum first-order quadrupole frequency shift with respect to the Larmor frequency for one satellite transition.

Eq. (1.50) is now the commonly used definition of the quadrupole frequency for half-integer spin nuclei in the field of NQR. But for $I = 1$ nuclei no notational consistency exists, and other definitions of ν_Q can be found [16]. Some differing definitions exist in the literature also for half-integer spin nuclei. For a comparison, we apply Abragam's definitions of ν_Q, Eq. (1.50), and the corresponding angular dependent definitions of ν'_Q and ω'_Q from Eq. (1.58). Then we use ω^*_Q or ν^*_Q in place of the various definitions used by the below-mentioned authors. The result is $\nu_\mathrm{Q} = 6\nu^*_\mathrm{Q}$ by Amoureux and Pruski [17], p. 145, $\nu_\mathrm{Q} = 2\omega^*_\mathrm{Q}$ by Deschamps and Massiot [18], p.187; $\omega'_\mathrm{Q} = 2\omega^*_\mathrm{Q}$ by Man [19], p. 8, and by Ashbrook and Wimperis [3], p. 48; and in the past, $\nu'_\mathrm{Q} = 3\nu^*_\mathrm{Q}$ by Frydman and coworker [20], p. 5375; and $\omega'_\mathrm{Q} = 6\omega^*_\mathrm{Q}$ by Samoson *et al*. [21], Nielsen *et al*. [22] and Veeman [23].

The quadrupole interaction can be regarded as a scalar product of two irreducible tensor operators of rank two [12], the tensor of the electric field gradient and the quadrupole tensor; see Eq. (1.16). Using this notation the quadrupole interaction is described by

$$\mathcal{H}_{\mathrm{Q}} = \frac{eQ}{2I(2I-1)} \sum_{m=-2}^{+2} (-1)^m T_m^{(2)} V_{-m}^{(2)} \ , \tag{1.51}$$

where

$$T_0^{(2)} = \tfrac{1}{\sqrt{6}}[3I_z^2 - I(I+1)], \quad T_{\pm1}^{(2)} = \tfrac{1}{\sqrt{2}}(I_{\pm1}I_z + I_z I_{\pm1}), \quad T_{\pm2}^{(2)} = (I_{\pm1})^2, \tag{1.52}$$

$$I_{\pm1} = \mp \tfrac{1}{\sqrt{2}} I_{\pm}, \tag{1.53}$$

and, in the principle axis system (PAS) of the electric field gradient tensor,

$$V_0^{(2)\,\mathrm{PAS}} = \sqrt{\tfrac{3}{2}}\, V_{ZZ} \ = \sqrt{\tfrac{3}{2}}\, eq, \quad V_{\pm1}^{(2)\,\mathrm{PAS}} = 0\,, \quad V_{\pm2}^{(2)\,\mathrm{PAS}} = \tfrac{1}{2}\, V_{ZZ}\, \eta = \tfrac{1}{2}\, \eta\, eq. \tag{1.54}$$

The transformation from the PAS (X, Y, Z) to the laboratory axis system (LAB) or to any arbitrary frame (x, y, z) can be performed by three successive rotations: α about the Z-axis, β about the obtained y'-axis, and γ about the z-axis. For the new $V_0^{(2)}$ component we revise Eq. (1.09) in light of Eq. (1.12) and Table 1.1 to

$$V_0^{(2)\mathrm{LAB}} = \sqrt{\tfrac{3}{2}}\ V_{ZZ} \left(\tfrac{3\cos^2\beta - 1}{2} + \tfrac{\eta}{2}\sin^2\beta\, \cos 2\alpha\right) = \sqrt{\tfrac{3}{2}}\ eq \left(\tfrac{3\cos^2\beta - 1}{2} + \tfrac{\eta}{2}\sin^2\beta\, \cos 2\alpha\right), \tag{1.55}$$

which is needed for the part of $\mathcal{H}_{\mathrm{Q}}$ that commutes with the Zeeman Hamiltonian I_z. This part is denoted by

$$\mathcal{H}_{\mathrm{Q}}^{(0)} = \tfrac{eQ}{2I(2I-1)} T_0^{(2)} V_0^{(2)} = \tfrac{eQ\, V_{ZZ}}{4I(2I-1)} [3I_z^2 - I(I+1)] \left(\tfrac{3\cos^2\beta - 1}{2} + \tfrac{\eta}{2}\sin^2\beta\, \cos 2\alpha\right). \tag{1.56}$$

By substituting $V_{ZZ} = eq$ and using Eq. (1.47) we obtain

$$\mathcal{H}_{\mathrm{Q}}^{(0)} = \tfrac{\hbar\omega_{\mathrm{Q}}}{6} \left(\tfrac{3\cos^2\beta - 1}{2} + \tfrac{\eta}{2}\sin^2\beta\, \cos 2\alpha\right) [3I_z^2 - I(I+1)]. \tag{1.57}$$

Given the angular dependent quadrupole frequency

$$\omega'_{\mathrm{Q}} = \omega_{\mathrm{Q}} \left(\frac{3\cos^2\beta - 1}{2} + \frac{\eta}{2}\sin^2\beta\, \cos 2\alpha\right), \tag{1.58}$$

one can write

$$\mathcal{H}_{\mathrm{Q}}^{(0)} = \frac{\hbar\, \omega'_{\mathrm{Q}}}{6} \big(3I_z^2 - I(I+1)\big). \tag{1.59}$$

In the interaction representation we have instead of Eq. (1.51),

$$\mathcal{H}_{\mathrm{Q,i}} = \frac{eQ}{2I(2I-1)} \sum_{m=-2}^{+2} (-1)^m T_m^{(2)} V_{-m}^{(2)} \exp(\mathrm{i}q\omega_{\mathrm{c}}t). \tag{1.60}$$

Using the Magnus expansion [12], we obtain similarly to Eq. (1.59) the first-order contribution,

$$\overline{\mathcal{H}_{\mathrm{Q}}^{(0)}} = \frac{\hbar\omega_{\mathrm{Q}}'}{6}\left(3I_z^2 - I(I+1)\right). \tag{1.61}$$

From the second-order contribution, the secular part with respect to I_z is

$$\overline{\mathcal{H}_{\mathrm{Q\,sec}}^{(1)}} = -\frac{\hbar\omega_{\mathrm{Q}}^2}{9\omega_{\mathrm{L}}}\left[2I_z\left(2I_z^2 - I(I+1) + \frac{1}{4}\right)\frac{V_{-1}V_{+1}}{V_{ZZ}^2} + I_z\left(I_z^2 - I(I+1) + \frac{1}{2}\right)\frac{V_{-2}V_2}{V_{ZZ}^2}\right]. \tag{1.62}$$

The irreducible tensor components in the laboratory axis system (LAB) or in any arbitrary frame (x, y, z)can be expressed by the principle axis components using

$$V_{\mathrm{Q}}^{(2)\mathrm{LAB}} = \sum_{m'=-2}^{+2} D_{m'm}^{(2)}(\alpha,\beta,\gamma)V_{\mathrm{PAS}\,m'}^{(2)}. \tag{1.63}$$

Quadrupole powder patterns of half-integer nuclei with first-order and second-order quadrupole interaction have already been calculated for a symmetric field gradient by Bloembergen, as presented in the review of Cohen and Reif [24]. Spectra describing the combined effect of quadrupole interactions and chemical shifts were first presented by Jones *et al*. [25]. A review of powder spectra in NMR and EPR was given by Taylor *et al*. [26] in 1975. For stronger quadrupole interactions, which cannot be described by perturbation theory, the eigenvalue problem of the full Hamiltonian has to be solved. Barnes *et al*. [27] briefly reviewed the work in this field performed up until 1988, when the standard assumption or condition was that the quadrupole and chemical shift tensors be coincident. Examples of low-symmetry sites that do not meet this condition were studied by Cheng *et al*. [28], Power *et al*. [29] and Skibsted *et al*. [30] describing the line shapes of ^{85,87}Rb in rubidium salts, ^{133}Cs in cesium chromate and ^{51}V MAS spectra, respectively.

An effective procedure for the powder average was introduced by Alderman *et al*. [31]. This approach provides a very fast simulation of powder patterns since, first, the intensity for a special orientation is averaged over the next-nearest orientations, and second, the time-consuming calculation of trigonometric functions could be replaced by simple division. Extensions by Sethi *et al*. [32] and Zheng *et al*. [33] allow the computation of centerband and sideband intensities of the central transition for any angle and speed.

The **first-order quadrupole powder pattern** can be obtained with $\mathcal{H} = \overline{\mathcal{H}_{\mathrm{Q}}^{(0)}}$ from Eq. (1.61) by assuming the resonance offset to be zero. Then, the first-order frequency shift becomes, with Eq. (1.58),

$$\nu_{m,m+1} - \nu_{\mathrm{L}} = \nu_{\mathrm{Q}}\left(\frac{3\cos^2\beta - 1}{2} + \frac{\eta}{2}\sin^2\beta\,\cos 2\alpha\right)\left(m + \frac{1}{2}\right) = \nu_{\mathrm{Q}}'\left(m + \frac{1}{2}\right). \tag{1.64}$$

The central transition corresponds to $m = -\frac{1}{2}$ and is not shifted by the first-order interaction.

In order to calculate the line shape one has to make assumptions about the excitation; see Section 2. Here we limit the considerations to nonselective excitation and have for a $\frac{\pi}{2}$-pulse in the y-direction $\rho = -I_x$. Fig. 1.2 gives some examples of the line shapes of random powders. The theoretical line shape is slightly Gaussian-broadened, in order to avoid singularities. The line at the Larmor frequency due to the central transition is cut off. It can be seen in Fig. 1.2 that the spectral width of a first-order quadrupole-broadened spectrum amounts to $\nu_{\mathrm{Q}}(2I-1)$. Magic-angle spinning (MAS) eliminates the first-order quadrupole broadening, if the MAS frequency is larger than the spectral width. In the case in which the spinning frequency is much smaller than the spectral width, we obtain spinning sideband spectra with envelopes corresponding to the static spectra in Fig. 1.2.

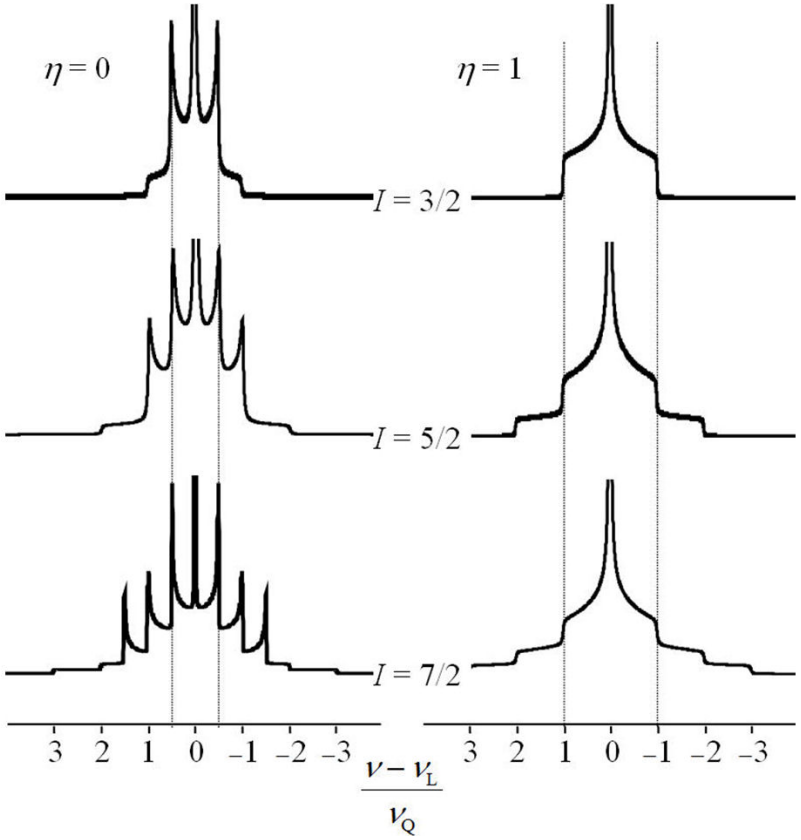

Figure 1.2. Examples of the static line shape (without MAS) of first-order quadrupole-broadened powder spectra for non-selective excitation. The signal of the central transition is not fully displayed (cut off).

The **second-order quadrupole powder pattern** can be obtained with $\mathcal{H} = \overline{\mathcal{H}_{\mathrm{Q}}^{(1)}}$ from Eq. (1.62). The calculation based on Eq. (1.35) of $\left(\mathcal{H}_{\mathrm{m+1,m+1-}}\mathcal{H}_{\mathrm{m,m}}\right)/\hbar$ (see) yields with zero-offset for single-quantum transitions

$$\nu_{m,m+1} - \nu_{\mathrm{L}} = -\frac{\nu_{\mathrm{Q}}^2}{18\,\nu_{\mathrm{L}}}\begin{Bmatrix}[24m(m+1) - 4I(I+1) + 9]V_{+1}V_{-1}\\ +[6m(m+1) - 2I(I+1) + 3]V_{+2}V_{-2}\end{Bmatrix}. \tag{1.65}$$

For symmetric (single and multiple) quantum transitions, we obtain

$$\nu_{m,-m} - \nu_{\mathrm{L}} = -\frac{m\,\nu_{\mathrm{Q}}^2}{9\,\nu_{\mathrm{L}}}\begin{Bmatrix}[4I(I+1) - 8m^2 - 1]V_{+1}V_{-1}\\ +[2I(I+1) - 2m^2 - 1]V_{+2}V_{-2}\end{Bmatrix}. \tag{1.66}$$

The components V_j are given in LAB notation. Using Wigner matrices of rank 2, they can be described as functions of the corresponding values in the PAS notations, which are given in Eq. (1.54). The products V_jV_{-j} in Eqs. (1.65) and (1.66) can also be written as Wigner matrices of ranks as high as 4. It is possible to express the products V_jV_{-j} in LAB (also via the system of the spinning rotor and the time-average of about one rotation period) in terms of PAS with a function g of the Euler angles α, β and the asymmetry parameter η:

$$g(\alpha,\beta,\eta) = A(\alpha,\eta)\cos^4\beta + B\,(\alpha,\eta)\cos^2\beta + C(\alpha,\eta). \tag{1.67}$$

Samoson [34] split the second-order quadrupole shift into an isotropic part (iso) describing the quadrupole shift of the center of gravity of the signal and an angular-dependent anisotropic part describing the quadrupole broadening of the signal:

$$\nu_{m,m+1} - \nu_{\mathrm{L}} = \nu_{\mathrm{iso}} + \nu(\alpha,\beta,\eta)$$

$$= -\frac{\nu_{\mathrm{Q}}^2}{6\,\nu_{\mathrm{L}}} \left\{ \begin{array}{l} \frac{1}{5}[I(I+1) - 9m(m+1) - 3]\left(1 + \frac{\eta^2}{3}\right) \\ + \left[I(I+1) - \frac{17}{3}m(m+1) - \frac{13}{6}\right] g(\alpha,\beta,\eta) \end{array} \right\}. \qquad (1.68)$$

This separation is very useful, since the isotropic shift corresponds to the center of gravity of the second-order quadrupole-broadened signal. The powder average about the function $g(\alpha,\beta,\eta)$ is zero, as can be shown using the functions in Table 1.2 and performing the corresponding integrations. The terms A, B, and C for Eq. (1.67) are given in Table 1.2 for the static case (no sample rotation) and for the case of fast magic-angle spinning. Similar terms for the static case were first presented by Narita *et al*. [35] with special Euler angles and rewritten by Baugher *et al*. [36] for the Euler angles that are used here. Similar terms for MAS were first given by Müller [37]. Both sources provide the sum of isotropic and anisotropic contributions, whereas Table 1.2 presents the anisotropic contribution with the powder average of zero. The original equation g by Samoson [34] contains printing mistakes in three terms.

Table 1.2. Functions A, B, and C in the equation $g(\alpha,\beta,\eta) = A(\alpha,\eta)\cos^4\beta + B\,(\alpha,\eta)\cos^2\beta + C(\alpha,\eta)$, Eq. (1.67), for the anisotropic part of the second-order line shapes of single-quantum transitions for static and MAS conditions.

Function	Static case	MAS
A	$-\frac{27}{8} - \frac{9}{4}\eta\cos 2\alpha - \frac{3}{8}\eta^2\cos^2 2\alpha$	$\frac{21}{16} - \frac{7}{8}\eta\cos 2\alpha + \frac{7}{48}\eta^2\cos^2 2\alpha$
B	$\frac{15}{4} - \frac{1}{2}\eta^2 + 2\eta\cos 2\alpha + \frac{3}{4}\eta^2\cos^2 2\alpha$	$-\frac{9}{8} + \frac{1}{12}\eta^2 + \eta\cos 2\alpha - \frac{7}{24}\eta^2\cos^2 2\alpha$
C	$-\frac{23}{40} + \frac{14}{15}\eta^2 + \frac{1}{4}\eta\cos 2\alpha - \frac{3}{8}\eta^2\cos^2 2\alpha$	$\frac{9}{80} - \frac{1}{15}\eta^2 - \frac{1}{8}\eta\cos 2\alpha + \frac{7}{48}\eta^2\cos^2 2\alpha$

We obtain identic results from Eqs. (1.65) and (1.66) if we insert the quantum number $m = -1/2$ for the central transition. The square brackets in Eqs. (1.65), (1.66) and (1.68) are then multiples of $\left[I(I+1) - \frac{3}{4}\right]$ and the result is

$$\nu_{-1/2,1/2} - \nu_{\mathrm{L}} = -\frac{\nu_{\mathrm{Q}}^2}{6\,\nu_{\mathrm{L}}}\left[I(I+1) - \frac{3}{4}\right]\left\{\frac{1}{5}\left(1 + \frac{\eta^2}{3}\right) + g(\alpha,\beta,\eta)\right\} \qquad (1.69)$$

with $g(\alpha,\beta,\eta)$ as g_{static} or g_{MAS} from Table 1.2. The first summand and $g(\alpha,\beta,\eta)$ in the curly brackets of Eq. (1.69) describe the isotropic and anisotropic contribution, respectively. In Fig. 1.3 we show some examples of second-order quadrupole-broadened powder spectra (random powder) of the central transition, without sample spinning (static) and with MAS.

Fig. 1.3 uses the scaling factor

$$A = \frac{\nu_{\mathrm{Q}}^2}{16\,\nu_{\mathrm{L}}}\left[I(I+1) - \frac{3}{4}\right], \qquad (1.70)$$

which was introduced by Cohen and Reif [24] as a convenient measure for the width of the second-order broadened spectrum. It should not be confused with function A in Eq. (1.67). On this scale, the spectral width for the MAS spectra is $72\,A/63$ and $98\,A/63$ for η = 0 and 1, respectively, in comparison to $25\,A/9$ and $40\,A/9$ for the static spectra at η = 0 and 1, respectively.

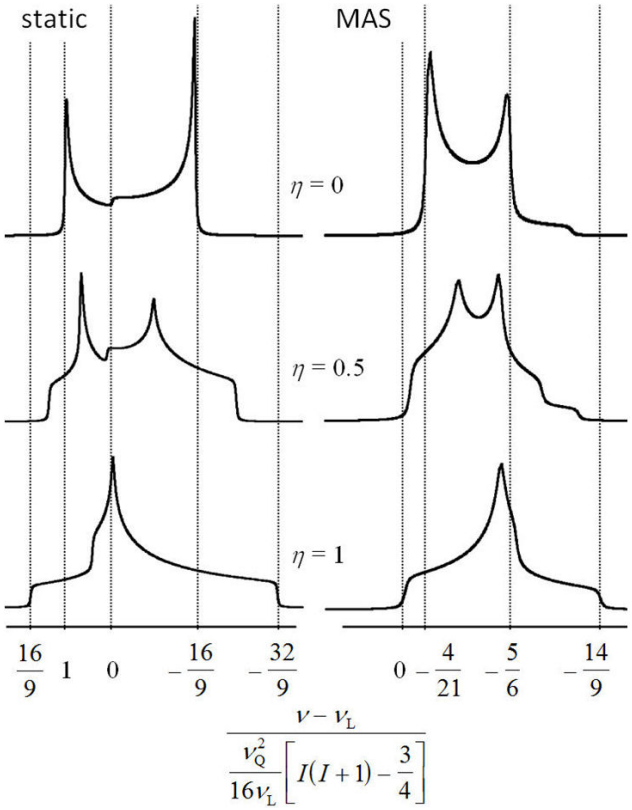

Fig. 1.3. Examples of the line shapes, static and with MAS, of second-order quadrupole-broadened powder spectra of the central transition. The theoretical line shapes are slightly Gaussian broadened.

In order to deduce the quadrupole parameters from experimentally obtained MAS spectra, it is usual to fit the experimental spectrum with calculated spectra using a utility program adapted to the spectrometer software. The freely accessible program dmfit by Massiot *et al.* [38] is widely used for the simulation of quadrupole broadening of NMR signals. For a rough estimation we introduce, using (Eq. 1.69), the angular frequency of the isotropic second-order quadrupole shift of the central transition,

$$\Delta\omega_{\mathrm{iso}} = \omega_{\mathrm{iso}} - \omega_{\mathrm{L}} = -\frac{\omega_{\mathrm{Q}}^2}{30\,\omega_{\mathrm{L}}}\left[I(I+1) - \frac{3}{4}\right]\left(1 + \frac{\eta^2}{3}\right), \tag{1.71}$$

and we obtain [39] for the second moment of the line shape with respect to the center of gravity for the static sample,

$$M_2 = \frac{23}{7}(\Delta\omega_{\mathrm{iso}})^2. \tag{1.72}$$

In the case of MAS with a spinning speed larger than the second-order broadening of the central transition, neglecting spinning sidebands, the result is

$$M_2{}^{\mathrm{MAS}} = \frac{1}{4}(\Delta\omega_{\mathrm{iso}})^2. \tag{1.73}$$

From Eqs. (1.72) and (1.73) it is found that the factor

$$\sqrt{\frac{M_2}{M_2^{\mathrm{MAS}}}} = \sqrt{\frac{92}{7}} \approx 3.6 \tag{1.74}$$

describes the reduction of the second-order line broadening by means of MAS [39].

Eq. (1.72) allows the estimation of the isotropic quadrupole shift, $\Delta\omega_{\mathrm{iso}}$ or $\Delta\nu_{\mathrm{iso}}$, from the *fwhm*, $\delta\nu_{1/2}$, of the MAS signal under the conditions that the signal is exclusively broadened by second-order quadrupole interaction and that the line shape can be approximated by a Gaussian line. Then the application of Eq. (1.91), see below, gives in connection with Eq. (1.74)

$$\Delta\nu_{\mathrm{iso}} = \sqrt{\frac{1}{\ln 4}}\ \delta\nu_{1/2}\ . \tag{1.75}$$

This means that the isotropic shift amounts to 0.85-fold of the *fwhm* of the MAS signal. The minus-sign in Eq. (1.71) means that the isotropic quadrupole shift decreases the resonance frequency and accordingly shifts the signal position to the right side on the ppm-scale.

The use of different symmetric transitions is the basis of multiple-quantum MAS NMR spectroscopy. We introduce the quantum level p. Symmetric coherences then have the notation $p/2 \leftrightarrow -p/2$ instead of $m \leftrightarrow -m$. The central transition corresponds to $p = -1$. Amoureux *et al*. [40, 41] calculated the shifts of the symmetric transition in the case of very fast sample rotation around the magic-angle $\theta_{\mathrm{m}} = \arccos 3^{-1/2} \approx 54.74°$. In that case, the contributions from the rank 2 components disappear and the rank 4 components give in our notation

$$\begin{aligned}\nu_{p/2,-p/2} - \nu_{\mathrm{L}} &= \nu^{\mathrm{iso}}(p) + \nu(p,\alpha,\beta,\eta)\\ &= \frac{p\,\nu_{\mathrm{Q}}^2}{6\,\nu_{\mathrm{L}}}\left\{\begin{array}{c}\frac{1}{5}\left[I(I+1) - \frac{3}{4}p^2\right]\left(1+\frac{\eta^2}{3}\right)\\ -\left[I(I+1) - \frac{17}{36}p^2 - \frac{5}{18}\right]\left\{-\frac{18}{7}P_4(\cos\theta)\right\} g_{\mathrm{MAS}}(\alpha,\beta,\eta)\end{array}\right\}.\end{aligned} \tag{1.76}$$

The anisotropic contribution (bottom in Eq. 1.76) is again described by the function $g_{\mathrm{MAS}}(\alpha,\beta,\eta)$; see Table 1.2. But the rank 4 contribution still contains the fourth Legendre polynomial

$$P_4(\cos\theta) = \tfrac{1}{8}(35\cos^4\theta - 30\cos^2\theta + 3) \tag{1.77}$$

as a function of the rotation angle. We can insert here the magic angle with $\cos\theta_{\mathrm{m}} = 1/\sqrt{3}$ and obtain $P_4(\cos\theta_{\mathrm{m}}) = -7/18$. Then, the value of the smaller curly bracket in Eq. (1.76) becomes 1, and disappears as a factor. This form is the fundamental equation for the MQMAS NMR spectroscopy of quadrupolar nuclei with half-integer spins.

However, we can insert instead of the magic angle one of the second angles for double rotation (DOR), $\theta = \arccos\sqrt{\left(6 \pm \sqrt{96/5}\right)/14} \approx 30.56°$ or $70.12°$. Then the Legendre polynominal P_4 in Eq. (1.76) is equal to zero and the total anisotropic part disappears. This is the fundamental scheme for DOR NMR.

1.5 Magnetic Dipolar Interaction between Nuclei

We have N number of nuclei in the sample and consider the dipolar interaction of a selected nucleus i, where $i = 1, 2, \ldots, N$, with any other nucleus defined as k, where $k \neq i = 1, 2, \ldots, N$.
The Hamiltonian, describing the interaction between the magnetic moments of the two nuclei with the distance $\boldsymbol{r}_{ik}$ is

$$\mathcal{H}_{\mathrm{D}} = -\frac{\mu_0}{4\pi}\frac{\gamma_i\gamma_k\hbar^2}{r_{ik}^3}\left(\frac{3(\boldsymbol{I}_i\cdot\boldsymbol{r}_{ik})(\boldsymbol{I}_k\cdot\boldsymbol{r}_{ik})}{r_{ik}^2} - \boldsymbol{I}_i\cdot\boldsymbol{I}_k\right). \tag{1.78}$$

Using the irreducible tensor notation one may write [12, 14]

$$\mathcal{H}_{\mathrm{D}} = C_{\mathrm{D}}^{ik}\sum_{q=-2}^{+2}(-1)^q T_q^{(2)}V_{-q}^{(2)}, \tag{1.79}$$

where we have generally

$$C_{\mathrm{D}}^{ik} = -\tfrac{\mu_0}{2\pi}\gamma_i\gamma_k\hbar^2$$

and for a coordinate system with z-axis parallel to $\boldsymbol{r}_{ik}$,

$$T_0^{(2)} = \tfrac{1}{\sqrt{6}}\left(3I_{z,i}I_{z,k} - \boldsymbol{I}_i\cdot\boldsymbol{I}_k\right),\quad T_{\pm1}^{(2)} = \tfrac{1}{\sqrt{2}}\left(I_{\pm1,i}I_{z,k} + I_{z,i}I_{\pm1,k}\right),\quad T_{\pm2}^{(2)} = I_{\pm1,i}I_{\pm1,k},$$

$$I_{\pm1} = \mp\tfrac{1}{\sqrt{2}}\,I_{\pm},\quad V_0^{(2)} = \sqrt{\tfrac{3}{2}}\,r_{ik}^{-3},\quad V_{\pm1}^{(2)} = 0\,,\quad V_{\pm2}^{(2)} = 0\,. \tag{1.80}$$

For **homonuclear dipolar interaction** (like spins I), $\gamma_i = \gamma_k = \gamma$, the part of $\mathcal{H}_{\mathrm{D}}$ commuting with $\gamma_i I_{z,i} + \gamma_k I_{z,k}$ for a pair (i,k) of spins with the distance $\boldsymbol{r}_{ik}$ [1] is

$$\mathcal{H}_{\mathrm{D}}^{(0)} = -\frac{\mu_0}{4\pi}\frac{\gamma^2\hbar^2}{2r_{ik}^3}(3\cos^2\beta_{ik} - 1)\left(3I_{z,i}I_{z,k} - \boldsymbol{I}_i\cdot\boldsymbol{I}_k\right). \tag{1.81}$$

For **heteronuclear dipolar interaction** (unlike spins S), $\gamma_i \neq \gamma_k$, we have

$$\mathcal{H}_{\mathrm{D}}^{(0)} = -\frac{\mu_0}{4\pi}\frac{\gamma_i\gamma_k\hbar^2}{2r_{ik}^3}(3\cos^2\beta_{ik} - 1)\;2S_{z,i}S_{z,k}. \tag{1.82}$$

I, S denote the spins of the resonant and non-resonant nuclei, respectively. The second moment (powder average) of the corresponding line shape is given in Ref. [1] for like spins in the case that the dipolar interaction of a spin pair with the distance r_{ik} is large compared with the quadrupole interaction:

$$M_2^{\mathrm{II}} = \frac{9}{5}\left(\frac{\mu_0}{4\pi}\gamma_{\mathrm{I}}^2\hbar\right)^2\frac{I(I+1)}{3}\frac{1}{r_{ik}^6}. \tag{1.83}$$

For unlike spins, the second moment is [1]

$$M_2^{\mathrm{IS}} = \frac{4}{5}\left(\frac{\mu_0}{4\pi}\gamma_{\mathrm{I}}\gamma_{\mathrm{S}}\hbar\right)^2\;\frac{S(S+1)}{3}\frac{1}{r_{ik}^6}. \tag{1.84}$$

The total second moment of the type-I spins is $M_2 = M_2^{\mathrm{II}} + M_2^{\mathrm{IS}}$. The latter heteronuclear contribution to the second moment remains the same, if a strong quadrupole interaction is present [1]. In contrast, the quadrupole interaction can reduce the second moment of the contribution of the homonuclear dipole interaction, Eq. (1.83), if $\nu_{\mathrm{Q}}(2I-1)$ (first-order spectral width) becomes larger than the homonuclear dipolar broadening [1, 8]. Spin-flipping between different transitions is then prohibited, and the second moment decreases. The reduction is less than 20%, if the second-order broadening of the central transition, indicated by parameter A in Eq. (1.70), is still smaller than the homonuclear broadening. The reduction factor of the homonuclear contribution to the second moment becomes $4/9$, if A is much larger than the homonuclear dipolar broadening. This then means that the I-spins are hypothetical unlike spins that can be described by one gyromagnetic ratio γ_{I}; compare Eqs. (1.83) and (1.84).

The pure dipolar second moment of a spin system consisting of N resonant spins of type I (homonuclear interaction of spins with the distance r_{I}) and M non-resonant spins of type S (heteronuclear interaction of spins with the distance r_{S}) can be determined by the dimensionless equation

$$\frac{M_2/\mathrm{Hz}^2}{\left(\frac{\gamma_{\mathrm{I}}}{2\pi}\right)^2} = \frac{M_2/\mathrm{s}^{-2}}{\gamma_{\mathrm{I}}^2} = M_2/\mathrm{T}^2 = \frac{c_{\mathrm{I}}}{r_{\mathrm{I}}^6/\mathrm{m}^6} + \frac{c_{\mathrm{S}}}{r_{\mathrm{S}}^6/\mathrm{m}^6} \tag{1.85}$$

with

$$c_{\mathrm{I}} = \frac{3}{5} I(I+1) \left(\frac{\mu_0}{4\pi}\right)^2 \gamma_{\mathrm{I}}^2 \hbar^2, \tag{1.86}$$

$$c_{\mathrm{S}} = \frac{4}{15} S(S+1) \left(\frac{\mu_0}{4\pi}\right)^2 \gamma_{\mathrm{S}}^2 \hbar^2, \tag{1.87}$$

$$\frac{1}{r_{\mathrm{I}}^6} = \frac{1}{N} \sum_{i=1}^{N} \sum_{k \neq j}^{N} \frac{1}{r_{ik}^6}\,, \qquad \frac{1}{r_{\mathrm{S}}^6} = \frac{1}{N} \sum_{i=1}^{N} \sum_{k=1}^{M} \frac{1}{r_{ik}^6}\,. \tag{1.88), (1.89}$$

Eqs. (1.85)—(1.89) can be used for the calculation of the dipolar second moment.

Table 1.3 provides the coefficients C_{I} for a special dimensionless equation using the non-SI units Gauss and Ångström, where the second moment is given in G^2 units (and divided by G^2) and the distances r_{ik} is given in Å (and divided by Å) [42]:

$$M_2/\mathrm{G}^2 = \frac{C_{\mathrm{I}}}{r_{\mathrm{I}}^6/\mathrm{Å}^6} + \frac{C_{\mathrm{S}}}{r_{\mathrm{S}}^6/\mathrm{Å}^6} \;=\; M_2/\mathrm{T}^2 \times 10^{-8} \tag{1.90}$$

The value C_{S} of a non-resonant nucleus can be easily calculated from the value of the same resonant nucleus C_{I} by $C_{\mathrm{S}} = C_{\mathrm{I}} \times 4/9$. The distances r_{I} and r_{S} denote in a simple model the internuclear distances of one resonant spin to another resonant spin and to a non-resonant spin, respectively. For the general case, r_{I} and r_{S} have to be calculated by means of Eqs (1.88) and (1.89), respectively.

Another dimensionless equation is very helpful, in order to correlate the second moment of a line, which is broadened by any interaction, to the line width, which is described by $fwhm \equiv \delta\nu_{1/2}$. Under the assumption of a Gaussian line shape, with T_2 as the transverse relaxation time in seconds and the line width $\delta\nu_{1/2}$ given in Hz, we obtain

$$M_2/\mathrm{s}^{-2} = \frac{2}{(T_2/\mathrm{s})^2} = \left(\delta\nu_{1/2}/\mathrm{Hz}\right)^2 \frac{\pi^2}{\ln 4} \approx 7.12 \times \left(\frac{\delta\nu_{1/2}}{\mathrm{Hz}}\right)^2 \text{ or } \frac{\delta\nu_{1/2}}{\mathrm{Hz}} \approx 0.3748 \times \sqrt{M_2/\mathrm{s}^{-2}}, \tag{1.91}$$

where M_2 has the unit s^{-2}: $M_2/\mathrm{s}^{-2} = \gamma_{\mathrm{I}}^2 \times M_2/\mathrm{T}^2 = \gamma_{\mathrm{I}}^2 \times 10^{-8} \times M_2/\mathrm{G}^2$.

Table 1.3. Values of C_I in Eq. (1.90) for some nuclei. Values of C_S can be obtained by C_S = 4/9 C_I. The gyromagnetic ratios were taken from Ref. [43].

nucleus	C_I	spin	$\gamma/10^7$ s^{-1}T^{-1}	nucleus	C_I	spin	$\gamma/10^7$ s^{-1}T^{-1}
^{1}H	358.167	1/2	26.7522128	^{63}Cu	126.559	3/2	7.1117890
^{2}H	22.5064	1	4.10662919	^{65}Cu	144.697	3/2	7.60435
^{7}Li	270.527	3/2	10.3977013	^{75}As	52.8599	3/2	4.596163
^{9}Be	35.3699	3/2	−3.759666	^{77}Se	13.1468	1/2	5.1253857
^{10}B	66.1705	3	2.8746786	^{79}Br	113.188	3/2	6.725616
^{11}B	184.411	3/2	8.5487044	^{81}Br	131.518	3/2	7.249776
^{13}C	22.6555	1/2	6.728284	^{87}Rb	193.178	3/2	8.786400
^{14}N	4.99055	1	1.9337792	^{93}Nb	712.306	9/2	6.5674
^{15}N	3.68250	1/2	10.136767	^{117}Sn	46.0144	1/2	−9.58879
^{17}O	76.8540	5/2	−3.62808	^{119}Sn	50.3634	1/2	−10.0317
^{19}F	317.343	1/2	25.18148	^{121}Sb	242.413	5/2	6.4435
^{23}Na	125.460	3/2	7.0808493	^{127}I	169.598	5/2	5.389573
^{27}Al	284.158	5/2	6.9762715	^{133}Cs	131.200	7/2	3.5332539
^{29}Si	14.1588	1/2	−5.3190	^{195}Pt	17.0596	1/2	5.8385
^{31}P	58.7999	1/2	10.8394	^{199}Hg	11.7516	1/2	4.8457916
^{35}Cl	17.2317	3/2	2.624198	^{201}Hg	8.00653	3/2	−1.788769
^{37}Cl	11.9395	3/2	2.184368	^{203}Tl	120.846	1/2	15.5393338
^{51}V	521.687	7/2	7.0455117	^{205}Tl	123.235	1/2	15.6921808
^{55}Mn	257.831	5/2	6.6452546	^{207}Pb	15.5850	1/2	5.58046
^{59}Co	421.373	7/2	6.332	^{209}Bi	316.108	9/2	4.3750

1.6 Anisotropy of the Chemical Shift

The Hamiltonian describing the anisotropic shielding (chemical shift anisotropy, CSA) in the principle axis system is [14]

$$\mathcal{H}_\mathrm{CSA} = C_\mathrm{CSA}\left[T_0^{(0)}V_0^{(0)} + \sum_{q=-2}^{+2}(-1)^q\, T_q^{(2)}V_{-q}^{(2)}\right] \tag{1.92}$$

with

$$T_0^{(0)} = \tfrac{1}{\sqrt{3}}\boldsymbol{I}_0\cdot\boldsymbol{B}_0,\ T_0^{(2)} = \sqrt{\tfrac{2}{3}}\,\boldsymbol{I}_0\cdot\boldsymbol{B}_0,\ T_{\pm1}^{(2)} = \tfrac{1}{\sqrt{2}}\boldsymbol{I}_{\pm1}\cdot\boldsymbol{B}_0\,,\ T_{\pm2}^{(2)} = 0,\ \boldsymbol{I}_{\pm1} = \mp\,\tfrac{1}{\sqrt{2}}\,\boldsymbol{I}_\pm,$$

$$V_0^{(0)} = -\tfrac{1}{\sqrt{3}}(\sigma_{XX}+\sigma_{YY}+\sigma_{ZZ}) = -\sqrt{3}\,\sigma_\mathrm{iso},\quad V_0^{(2)} = \sqrt{\tfrac{3}{2}}\,(\sigma_{ZZ}-\sigma_\mathrm{iso}) = \sqrt{\tfrac{3}{2}}\,\delta,$$

$$V_{\pm2}^{(2)} = \tfrac{1}{2}(\sigma_{XX}-\sigma_{YY}) = \tfrac{1}{2}\eta\,\zeta,\quad V_{\pm1}^{(2)} = 0,\quad C_\mathrm{CSA} = \gamma\,\hbar. \tag{1.93}$$

The shielding anisotropy factor $\zeta = \sigma_{ZZ} - \sigma_\mathrm{iso}$ should not be confused with the commonly used shielding anisotropy $\Delta\sigma = \sigma_{ZZ} - \frac{1}{2}(\sigma_{XX} + \sigma_{YY})$ which is $\Delta\sigma = \sigma_\parallel - \sigma_\perp$ for an axial symmetric tensor ($\eta = 0$). We have $\Delta\sigma = \frac{3}{2}\zeta$. IUPAC [44] recommends the use of the Greek lower case zeta, ζ, for the shielding anisotropy factor instead of the previously used δ, in order to avoid confusion with the parameter of the chemical shift. The isotropic shielding is $\sigma_\mathrm{iso} = \frac{1}{3}(\sigma_{XX} + \sigma_{YY} + \sigma_{ZZ})$ with σ_{XX}, σ_{YY}, σ_{ZZ} as the components of the shielding tensor in the principle axis system. We use the convention of Haeberlen [12] $|\sigma_{ZZ} - \sigma_\mathrm{iso}| \geq |\sigma_{XX} - \sigma_\mathrm{iso}| \geq |\sigma_{YY} - \sigma_\mathrm{iso}|$, which is recommended by the IUPAC [44]. This means that the ordering can be either $\sigma_{ZZ} \geq \sigma_{YY} \geq \sigma_{XX}$ or $\sigma_{ZZ} \leq \sigma_{YY} \leq \sigma_{XX}$

depending on the shielding tensor shape. The shielding asymmetry, η, with $0 \leq \eta \leq 1$ is in the Haeberlen notation

$$\eta = \frac{\sigma_{YY} - \sigma_{XX}}{\sigma_{ZZ} - \sigma_{\mathrm{iso}}}. \tag{1.94}$$

The Haeberlen notation follows the term ordering in the textbook of Abragam [1] (page 166 of the paperback edition), where $|V_{ZZ}| \geq |V_{XX}| \geq |V_{YY}|$ was defined for the electric field gradient tensor. But Abragam [1] claimed on the same page that $0 \leq \eta \leq 1$ is true for the asymmetry parameter $\eta = \frac{V_{XX} - V_{YY}}{V_{ZZ}}$. However, this can be fulfilled only for $|V_{ZZ}| \geq |V_{YY}| \geq |V_{XX}|$. Using Eq. (1.47) we follow the convention of Abragam [1], Slichter [45] and Ernst *et al*. [46] and use in opposition to Abragam [1] the ordering $|V_{ZZ}| \geq |V_{YY}| \geq |V_{XX}|$. As a result, we have a different ordering of the XX and YY terms for quadrupole interactions and chemical shifts.

After transformation to the laboratory frame (by means of the Euler angles α and β), the secular parts of both the isotropic and anisotropic contributions to the chemical shift are

$$\mathcal{H}_{\mathrm{CSA}}^{(0)\mathrm{LAB}} = \gamma\, \hbar\, B_0 I_z \left\{ -\sigma_{\mathrm{iso}} + \delta \left[\frac{3\cos^2\beta - 1}{2} + \frac{\eta}{2} \sin^2\beta\, \cos 2\alpha \right] \right\}. \tag{1.95}$$

The spectra of powder samples, which are broadened by chemical shift anisotropy, are called "CSA powder patterns", see [47], page 31. We can again use the second moment to describe line broadening by CSA. With $\Delta\sigma = \sigma_{ZZ} - \frac{1}{2}(\sigma_{XX} + \sigma_{YY})$ we have

$$M_2^{\mathrm{CSA}} = \frac{4}{9} \frac{(\Delta\sigma\, \omega_{\mathrm{L}})^2}{5} \left(1 + \frac{\eta^2}{3} \right). \tag{1.96}$$

1.7 Knight Shift

Walter Knight found in 1949 that the resonance frequency of ^{63}Cu in metallic copper occurred at a 1.0023-fold (shift of 2300 ppm) frequency with respect to the frequency for diamagnetic CuCl [48]. The cause of this shift is a hyperfine interaction of the nucleus with the conducting electrons. Charles Slichter described the Knight shift on pages 113−127 of his textbook [45] by four specifics: The shift is with few exceptions positive; the relative shift is, like the chemical shift, unaffected by the external magnetic field; the shift is nearly independent of temperature; and the shift increases in general with increasing nuclear charge Z.

For the estimation of the Knight shift we introduce the per-atom Pauli spin susceptibility, χ_{P} (The value χ_{P} in this definition has to be multiplied by the volume of an atom, V_{a}, if the common definition of the susceptibility per unit volume is used.). The Pauli spin susceptibility refers to the susceptibility of the electrons at the Fermi surface in the conductivity band and is only a part of the total electron spin susceptibility [49]. We also use the averaged value of the square of the wave function, $\langle|\psi(0)|^2\rangle$, at the radius $r = 0$ for the s-electrons at the Fermi surface, which is essential for the hyperfine structure of the ESR spectra. The wave function is normalized for free atoms. Therefore, the quantity $\langle|\psi(0)|^2\rangle$, often denoted as P_{F}, can be considered as the average concentration of Fermi electrons at the nucleus in the metal divided by the corresponding value for a single free atom. Then the contact interaction term that describes the isotropic Knight shift is [49, 50]

$$K = \frac{\Delta B}{B} = \frac{\Delta\nu}{\nu} = \frac{8\pi}{3} \chi_{\mathrm{P}}\, \langle|\psi(0)|^2\rangle. \tag{1.97}$$

An anisotropic effect can also occur in noncubic metals. For crystals of axial symmetry, the anisotropic part of the Knight shift, K_{ax}, is a function of the angle θ between the rotational symmetry axis and the external magnetic field. The shape of the p-electron charge distribution with a dipole field at $r = 0$ is described by the function q_{F}. The anisotropic contribution to the Knight shift becomes [50]

$$K_{\mathrm{ax}} = \frac{\Delta B_{\mathrm{ax}}}{B} = \frac{\Delta \nu_{\mathrm{ax}}}{\nu} = q_{\mathrm{F}}\, \chi_{\mathrm{P}}\, (3\cos^2\theta - 1). \tag{1.98}$$

Knight shifts in cases of lower symmetry are described on page 63 of Carter *et al*. [49]. A weak isotope effect in the Knight shifts at the order of magnitude of 10^{-3} could be observed for isotopes of Li, Cu, Ga, Rb, and Hg; see [49] page 17. Table 1.4 shows that experimentally observed Knight shifts [49] vary only slightly between the two temperatures 4 K and 300 K.

NMR in metals has been described in reviews by Winter [51], Carter *et al*. [49] and van der Klink and Brom [52]. Molecules that are adsorbed on metallic particles show in their NMR spectra the Knight shift as well. Metal clusters consisting of 200–5000 atoms in supported catalysts can be characterized by the so-called adsorbate Knight shifts of the adsorbed molecules, mainly by ^{1}H NMR, but also by ^{2}H, ^{13}C and ^{129}Xe NMR; see the review by Khanra [53]. Babu *et al*. [54] investigated the ^{13}C NMR Knight shift in spectra of CO and CN adsorbed on 2.5-nm Pt particles that were supported on a conducting carbon electrode material.

Table 1.4. Knight shift data from Carter *et al.* [49], including the elements, the Knight shifts K at 300 K, the axial Knight shifts K_{ax} at 300 K and the corresponding values at 4 K in brackets.

Li	K = 0.026%		
Be	K = −0.0025%	$K_{\mathrm{ax}} < 0.0003\%$	
Na	K = 0.113%	(K = 0.107%)	
Mg	K = 0.112%	(K = 0.113%)	($K_{\mathrm{ax}} <$ 0.0002%)
Al	K = 0.164%	(K = 0.161%)	
K	K = 0.26%	(K = 0.25%)	
Sc	K = 0.253%	K_{ax} = −0.023%	
	(K = 0.29%)	(K_{ax} = −0.032%)	
Ti	(K = 0.4%)		
V	K = 0.580%	(K = 0.570%)	
Cr	K = 0.69%		
Mn-β	K = 0.375%	K_{ax} = −0.002%	
	(K = 0.39%)	(K_{ax} = −0.02%)	
Mn-α I	K = −4.7%		
Mn-α II	K = −2.1%		
Mn-α III	K = 0.05%		
Mn-α IV	K = 0.35%		
Cu	K = 0.2394%	(K = 0.238%)	
Zn	K = 0.20%		
Ga	K = 0.155%	K_{ax} = −0.007%	
	(K = 0.132%)	(K_{ax} = −0.009%)	
Rb	K = 0.651%	(K = 0.646%)	
Y	K = 0.352%	K_{ax} = −0.026	(K = 0.34%)
Nb	K = 0.87%	(K = 0.89%)	
Mo	K = 0.61%	(K = 0.59%)	
Tc	K = 0.72%	K_{ax} = 0.11%	
Rh	K = 0.412%	(K = 0.43%)	
Pd	K = −3.05%	(K = −4.10%)	
Ag	K = 0.525%	(K = 0.520%)	
Cd	K = 0.415%	K_{ax} = 0.016%	
	(K = 0.35%)	(K_{ax} = −0.003%)	
In	K = 0.82%	K_{ax} = −0.14%	
	(K = 0.81%)	(K_{ax} = −0.05%)	
Sn-β	K = 0.735%	K_{ax} = 0.025%	
	(K = 0.718%)	(K_{ax} = 0.029%)	
Te	K = −0.062%		
Cs	K = 1.49%	(K = 1.57%)	
Ba	K = 0.403%		
Ta	K = 1.1%		
W	K = 1.04%	(K = 1.04%)	
Re	(K = 1.02%)	($K_{\mathrm{ax}} < 0.2\%$)	
Ir	(K = 1.3%)		
Pt	K = −2.918%	(K = −3.44%)	
Au	(K = 1.65%)		
Hg	K = 2.72%	(K = 2.68%)	(K_{ax} = −0.140%)
Tl	K = 1.55%	(K = 1.65%)	(K_{ax} = −0.050%)
Pb	K = 1.50%	(K = 1.46%)	
Wi	(K = −1.25%)	(K_{ax} = −0.3%)	

1.8 Literature

[1] A. Abragam, Principles of Nuclear Magnetism (paperback reprint 1989), Oxford University Press, Oxford, 1961.

[2] O. Glotova, N. Ponamareva, N. Sinyavsky, B. Nogaj, Non-cyclic Geometric Phase of Nuclear Quadrupole Resonance Signals of Powdered Samples, Solid State Nucl. Magn. Reson. 39 (2011) 1-6.

[3] S.E. Ashbrook, S. Wimperis, Quadrupolar Coupling: An Introduction and Crystallographic Aspects, in: R.E. Wasylishen, S.E. Ashbrook, S. Wimperis (Eds.) NMR of Quadrupolar Nuclei in Solid Materials, Vol., Wiley, Chichester, 2012, pp. 45-62.

[4] M. Weissbluth, Atoms and Molecules, Academic Press, New York, London, 1978.

[5] E.P. Wigner, Gruppentheorie und ihre Anwendung auf die Quantenmechanik der Atomspektren Vieweg & Sohn, Braunschweig, 1931.

[6] D.A. Varshalovich, A.N. Moskalev, V.K. Khersanskii, Quantum Theory of Angular Momentum, World Scientific, Singapore, 1988.

[7] H. Goldstein, C. Poole, J. Safko, Euler Angles in Alternate Conventions, in: Classical Mechanics, Vol., Pearson at Addison-Wesley, San Francisco, 2002, pp. 601-605.

[8] D. Freude, J. Haase, Quadrupole Effects in Solid-State NMR, NMR Basic Principles and Progress 29 (1993) 1-90.

[9] M.A. Morrison, G.A. Parker, A Guide to Rotations in Quantum-mechanics, Austr. J. Phys. 40 (1987) 465-497.

[10] P.P. Man, Wigner Active and Passive Rotation Matrices Applied to NMR Tensor, Concepts Magn. Reson. Part A 45A (2017) e21385.

[11] M.E. Rose, Elementary Theory of Angular Momentum, J. Wiley, Ney York, 1967.

[12] U. Haeberlen, High Resolution NMR in Solids, Selective Averaging, Academic Press, New York, San Francisco, London, 1976.

[13] K. Blum, Density Matrix Theory and Applications, Plenum Press, New York, 1981.

[14] M. Mehring, Principles of High Resolution NMR in Solids, Springer Verlag, Berlin, Heidelberg, New York, 1983.

[15] W. Magnus, On the Exponential Solution of Differential Equations for a Linear Operator, Commun. Pure and Appl. Math. 7 (1954) 649-673.

[16] G.L. Hoatson, R.L. Vold, ^{2}H-NMR Spectroscopy of Solids and Liquid Crystals, NMR Basic Principles and Progress 32 (1994) 1-67.

[17] J.-P. Amoureux, M. Pruski, MQMAS NMR: Experimental Strategies, in: R.E. Wasylishen, S.E. Ashbrook, S. Wimperis (Eds.) NMR of Quadrupolar Nuclei in Solid Materials, Vol., Wiley, Chichester, 2012, pp. 143-162.

[18] M. Deschamps, D. Massiot, Correlation Experiments Involving Half-integer Quadrupolar Nuclei, in: R.E. Wasylishen, S.E. Ashbrook, S. Wimperis (Eds.) NMR of Quadrupolar Nuclei in Solid Materials, Vol., Wiley, Chichester, 2012, pp. 179-198.

[19] P.P. Man, Quadrupolar Interactions, in: R.E. Wasylishen, S.E. Ashbrook, S. Wimperis (Eds.) NMR of Quadrupolar Nuclei in Solid Materials, Vol., Wiley, Chichester, 2012, pp. 3-16.

[20] A. Medek, J.S. Harwood, L. Frydman, Multiple-quantum Magic-angle Spinning NMR: A New Method for the Study of Quadrupolar Nuclei in Solids, J. Am. Chem. Soc. 117 (1995) 12779-12787.

[21] A. Samoson, E. Lippmaa, Central Transition NMR Excitation Spectra of Half-integer Quadrupole Nuclei, Chem. Phys. Lett. 100 (1983) 205-208.

[22] N.C. Nielsen, H. Bildsoe, H.J. Jakobsen, Multiple-quantum MAS Nutation NMR Spectroscopy of Quadrupolar Nuclei, J. Magn. Reson. 97 (1992) 149-161.

[23] W.S. Veeman, Quadrupole Nutation NMR in Solids, Z. Naturforsch. A 47 (1992) 353-360.

[24] M.H. Cohen, F. Reif, Quadrupole Effects in NMR Studies of Solids, Solid State Phys. 5 (1957) 321-438.

[25] W.H. Jones, T.P. Graham, R.G. Barnes, NMR Line Shapes Resulting from the Combined Effects of Nuclear Quadrupole and Anisotropic Shift Interactions, Phys. Rev. 132 (1963) 1898-1909.

[26] P.C. Taylor, J.F. Baugher, H.M. Kriz, Magnetic-Resonance Spectra in Polycrystalline Solids, Chem. Rev. 75 (1975) 203-240.

[27] R.G. Barnes, D.R. Torgeson, P.J. Bray, On NMR Powder Spectrum Simulation for Nuclei with $I>1/2$, Phys. Stat. Sol. 147 (1988) K175-K178.

[28] J.T. Cheng, J.C. Edwards, P.D. Ellis, Measurement of Quadrupolar Coupling Constants, Shielding Tensor Elements and the Relative Orientation of Tensor Principal Axis Systems for Rubidium-87 and Rubidium-85 Nuclei in Rubidium Salts by Solid-state NMR J. Phys. Chem. 94 (1990) 553-561.

[29] W.P. Power, R.E. Wasylishen, S. Mooibroek, B.A. Pettitt, W. Danchura, Simulation of NMR Powder Line Shapes of Quadrupolar Nuclei with Half-integer Spin at Low-symmetry Sites, J. Phys. Chem. 94 (1990) 5916-5918.

[30] J. Skibsted, N.C. Nielsen, H. Bildsoe, J. Jacobsen, ^{51}V MAS NMR Spectroscopy: Determination of Quadrupole and Anisotropic Shielding Tensors, Including the Relative Orientation of their Principal-axis Systems, Chem. Phys. Lett. 188 (1992) 405-412.

[31] D.W. Alderman, M.S. Solum, D.M. Grant, Methods for Analyzing Spectroscopic Line Shapes. NMR Solid Powder Pattern, J. Chem. Phys. 84 (1986) 3717-3725.

[32] N.K. Sethi, D.W. Alderman, D.M. Grant, NMR-spectra from Powdered Solids Spinning at Any Angle and Speed - Simulations and Experiments, Mol. Phys. 71 (1990) 217-238.

[33] Z.W. Zheng, Z.H. Gan, N.K. Sethi, D.W. Alderman, D.M. Grant, An Efficient Simulation of Variable-angle Spinning Lineshapes for the Quadrupolar Nuclei with Half-integer Spin, J. Magn. Reson. 95 (1991) 509-522.

[34] A. Samoson, Satellite Transition High-resolution NMR of Quadrupolar Nuclei in Powders, Chem. Phys. Lett. 119 (1985) 29-32.

[35] K. Narita, J.J. Umeda, H. Kusumoto, NMR Powder Patterns of the Second-order Nuclear-quadrupole Interaction on the Central Line in Solids with Asymmetric Field Gradient, J. Chem. Phys. 44 (1966) 2719-2723.

[36] J.F. Baugher, P.C. Taylor, T. Oja, P.J. Bray., NMR Powder Patterns in the Presence of Completely Asymmetric Quadrupole and Chemical Shift Effects: Application to Metavanadates, J. Chem. Phys. 50 (1969) 4914-4925.

[37] D. Müller, Zur Bestimmung Chemischer Verschiebungen der NMR-Frequenzen bei Quadrupolkernen aus den MAS NMR-Spektren, Ann. der Physik 39 (1982) 451-460.

[38] D. Massiot, F. Fayon, M. Capron, I. King, S. Le Calve, B. Alonso, J.O. Durand, B. Bujoli, Z.H. Gan, G. Hoatson, Modelling One- and Two-dimensional Solid-state NMR Spectra, Magn. Reson. Chem. 40 (2002) 70-76.

[39] D. Freude, J. Haase, J. Klinowski, T.A. Carpenter, G. Ronikier, NMR Line Shifts Caused by the Second-order Quadrupolar Interaction, Chem. Phys. Lett. 119 (1985) 365-367.

[40] J.P. Amoureux, C. Fernandez, Triple, Quintuple and Higher Orders Multiple Quantum MAS NMR of Quadrupolar Nuclei, Solid State Nucl. Magn. Reson. 10 (1998) 211-224.

[41] J.P. Amoureux, M. Pruski, Advances in MQMAS NMR, in: D.M. Grant, R.K. Harris (Eds.) Encyclopedia of Nuclear Magnetic Resonance, Vol. 9, John Wiley & Sons, Chichester, 2002, pp. 226-251.

[42] D. Freude, J. Kärger, NMR Techniques, in: F. Schüth, K. Sing, J. Weitkamp (Eds.) Handbook of Porous Materials, Vol. 1, Wiley-VCH, Chichester, 2002, pp. 465-505.

[43] R.K. Harris, E.D. Becker, S.M.C. De Menezes, R. Goodfellow, P. Granger, NMR Nomenclature. Nuclear Spin Properties and Conventions for Chemical Shifts - (IUPAC Recommendations 2001), Pure Appl. Chem. 73 (2001) 1795-1818.

[44] R.K. Harris, E.D. Becker, S.M.C. De Menezes, P. Granger, R.E. Hoffman, K.W. Zilm, Further Conventions for NMR Shielding and Chemical Shifts (IUPAC Recommendations 2008), Pure Appl. Chem. 80 (2008) 59-84.

[45] C.P. Slichter, Principles of Magnetic Resonance, Springer Verlag, Berlin, Heidelberg, New York, London, Paris, Tokyo, Hong Kong, 1990.

[46] R.R. Ernst, G. Bodenhausen, A. Wokaun, Principles of NMR in One and Two Dimensions, Oxford Univ. Press, London/New York, 1987.

[47] K. Schmidt-Rohr, H.W. Spiess, Multidimensional Solid-state NMR and Polymers, Academic Press, London, 1994.

[48] W.D. Knight, NMR Shift in Metals, Phys. Rev. 76 (1949) 1259-1260.

[49] G.C. Carter, L.H. Bennett, D.J. Kahan, Metallic Shifts in NMR, Pergamon Press, Oxford, New York, Toronto, Sydney, Paris, Frankfurt, 1977.

[50] W.D. Knight, S. Kobayashi, Knight Shift, in: D.M. Gran, R.K. Harris (Eds.) Encyclopedia of Nuclear Magnetic Resonance, Vol. 4, Wiley, Chichester, 1996, pp. 2672-2679.

[51] J. Winter, Magnetic Resonance in Metals, Oxford University Press, New York, 1971.

[52] J.J. van der Klink, H.B. Brom, NMR in Metals, Metal Particles and Metal Cluster Compounds, Progr. NMR Spectrosc. 36 (2000) 89-201.

[53] B.C. Khanra, Surface characterisation from adsorbate Knight shifts, Int. J. Mod. Phys. B 11 (1997) 1635-1668.

[54] P.K. Babu, E. Oldfield, A. Wieckowski, Nanoparticle Surfaces Studied by Electrochemical NMR, in: C.C. Vayenas, B.E. Conway, R.E. White (Eds.) Modern Aspects of Electrochemistry, Vol. 36, Kluwer Academic/Plenum Publishers, New York, 2003, pp. 1-50.